THE JOURNAL OF BIOLOGICAL CHEMISTRY VOL. 287, NO. 34, pp. 28386–28397, August 17, 2012

α-Galactosidase Aggregation Is a Determinant of Pharmacological Chaperone Efficacy on Fabry Disease Mutants*[S]

Received for publication, February 8, 2012, and in revised form, June 14, 2012 Published, JBC Papers in Press, July 6, 2012, DOI 10.1074/jbc.M112.351056

Aleksandra Siekierska[‡§¶], Greet De Baets[‡§¶], Joke Reumers[‡§], Rodrigo Gallardo[§¶], Stanislav Rudyak[‡§], Kerensa Broersen[‡§1], Jose Couceiro[§¶], Joost Van Durme[‡§¶], Joost Schymkowitz[§¶2], and Frederic Rousseau[§¶3]

From the [‡]Vrije Universiteit Brussel (VUB), Pleinlaan 2, 1050 Brussels, Belgium, the [§]VIB SWITCH Laboratory, Belgium, and the [¶]Department of Cellular and Molecular Medicine, University of Leuven, B-3000 Leuven, Belgium

Background: Deficiency in α-galactosidase activity leads to Fabry disease, for which treatment employing pharmacological chaperones is being developed.
Results: Aggregating α-galactosidase mutants are not responsive to the treatment with the pharmacological chaperone, 1-deoxygalactonojirimycin (DGJ).
Conclusion: Aggregation of α-galactosidase is a decisive factor for DGJ efficiency.
Significance: Combining pharmacological chaperones treatment with suppression of aggregation might be beneficial for future therapeutic strategy against Fabry disease.

Fabry disease is a lysosomal storage disorder caused by loss of α-galactosidase function. More than 500 Fabry disease mutants have been identified, the majority of which are structurally destabilized. A therapeutic strategy under development for lysosomal storage diseases consists of using pharmacological chaperones to stabilize the structure of the mutant protein, thereby promoting lysosomal delivery over retrograde degradation. The substrate analog 1-deoxygalactonojirimycin (DGJ) has been shown to restore activity of mutant α-galactosidase and is currently in clinical trial for treatment of Fabry disease. However, only ~65% of tested mutants respond to treatment in cultured patient fibroblasts, and the structural underpinnings of DGJ response remain poorly explained. Using computational modeling and cell culture experiments, we show that the DGJ response is negatively affected by protein aggregation of α-galactosidase mutants, revealing a qualitative difference between misfolding-associated and aggregation-associated loss of function. A scoring function combining predicted thermodynamic stability and intrinsic aggregation propensity of mutants captures well their aggregation behavior under overexpression in HeLa cells. Interestingly, the same classifier performs well on DGJ response data of patient-derived cultured lymphoblasts, showing that protein aggregation is an important determinant of chemical chaperone efficiency under endogenous expression levels as well. Our observations reinforce the idea that treatment of aggregation-associated loss of function observed for the more severe α-galactosidase mutants could be enhanced by combining pharmacological chaperone treatment with the suppression of mutant aggregation, *e.g.* via proteostatic regulator compounds that increase cellular chaperone expression.

Fabry disease (FD)[4] (OMIM 301500) is a metabolic X-linked inherited lysosomal storage disorder that results from the deficient activity of α-galactosidase A (α-Gal) (1). The protein α-Gal is a lysosomal hydrolase that cleaves neutral glycosphingolipids with terminal α-linked galactosyl moieties, mainly globotriaosylceramides (Gb3). A mouse knock-out model of FD showed accumulation of Gb3 in the liver and the kidneys (2). Similarly, patients with FD show progressive deposition of Gb3 in lysosomes and suffer from angikeratomas, acroparesthesis, hypohidrosis, and progressive vascular disease of the heart, kidneys, and central nervous system. This wide clinical spectrum is characteristic for the classic or early onset form of FD. However, there is also an atypical form of FD, mainly limited to heart disorders and diagnosed later in the life time, called variant or late onset FD (3). Human native α-Gal is a homodimer of ~100 kDa post-translationally modified to contain mannose oligosaccharide chains. The α-Gal subunit is synthesized as an inactive ~55-kDa precursor that undergoes maturation in endoplasmic reticulum (ER) and Golgi apparatus and is delivered to lysosomes as an ~50-kDa monomer where it forms a functional dimer (4, 5). More than 500 mutations have been identified in

* This work was supported by the Funds for Scientific Research of Flanders (FWO) and the Federal Office for Scientific Affairs, Belgium, Grant IUAP P6/43 (to the SWITCH Laboratory).
[S] This article contains a supplemental table.
[1] Present address: Faculty of Science and Technology, MIRA Institute for Biomedical Technology and Technical Medicine, University of Twente, The Netherlands.
[2] To whom correspondence may be addressed: SWITCH Laboratory, Dept. of Molecular Cell Biology, University of Leuven, B-3000 Leuven, Belgium. Tel.: 32-16-372573; Fax: 858-784-2779; E-mail: joost.schymkowitz@switch.vib-kuleuven.be.
[3] To whom correspondence may be addressed: SWITCH Laboratory, Dept. of Molecular Cell Biology, University of Leuven, B-3000 Leuven, Belgium. Tel.: 32-16-372572; Fax: 32-16-372751; E-mail: frederic.rousseau@switch.vib-kuleuven.be.

[4] The abbreviations used are: FD, Fabry disease; BFA, brefeldin A; Bis-Tris, bis(2-hydroxyethyl)iminotris(hydroxymethyl)methane; DGJ, 1-deoxygalactonojirimycin; ER, endoplasmic reticulum; α-Gal, α-galactosidase A; Gb3, globotriaosylceramide(s); LAMP1, lysosomal-associated membrane protein 1; MASS, Mutant Aggregation and Stability Spectrum; 4-MU-α-Gal, 4-methylumbelliferyl-α-D-galactopyranoside; SEC, size exclusion chromatography; RIPA, radioimmune precipitation assay; ERAD, ER-associated degradation.

the α-Gal gene including more than 300 missense mutations (Human Gene Mutation Database), the majority of which cause mild to severe structural defects.

Until recently, Fabry disease has been traditionally managed by symptomatic treatment. In 2001 it was shown that intravenous infusion of wild type protein to Fabry disease patients can reverse the major pathologic consequences of the disease (6–8). Two medications were approved for enzyme replacement therapy in FD: Replagal (gene-activated human agalsidase α) and Fabrazyme (recombinant human agalsidase β). A pharmacological chaperone 1-deoxygalactonojirimycin (DGJ) is currently in third phase of clinical trials. DGJ is a competitive inhibitor of α-Gal that in subinhibitory concentrations effectively enhances the mutant enzyme activity. By binding to its active site, DGJ chaperones unstable enzyme variants in the ER. This interaction increases the thermodynamic stability of the mutant enzyme and rescues it from misfolding in the neutral environment of the endoplasmic reticulum, allowing mutant α-Gal to pass through ER quality control, Golgi maturation, and being sorted into the lysosomes. Once in the lysosome, DGJ dissociates from α-Gal as a result of high substrate concentration and low pH environment (9, 10). DGJ binding to α-Gal introduces stabilizing interactions between the imino group on DGJ and several Asp in α-Gal (11, 12). However, a recent study addressing DGJ response of 75 α-Gal missense mutations in cultured lymphoblasts of Fabry disease patients (13) revealed that overall about 65% of mutants showed improved α-Gal activity and reduced Gb3 levels. Specifically, about half of the classic Fabry disease mutants were DGJ-responsive whereas 90% of the variant Fabry disease mutants showed significant improvement.

Mapping the mutations on the α-Gal structure, it turned out that the classic Fabry mutations are causing large structural perturbations and are generally located in functionally important regions, including the active site, whereas variant mutants are generally less severe (14, 15). Still, it remains very difficult to rationalize DGJ response solely from structural information (16) as only approximately 40% of nonresponsive mutants can be correctly predicted from structure alone (17). More robust prediction has been achieved recently by combining structural information with sequence conservation scoring (17, 18). The addition of position specific scoring matrices derived from paralogs, but excluding far homologs, allows predicting DGJ response with an accuracy above 80%. Although this approach provides a useful classifier of DGJ response, the use of implicit sequence information does not provide mechanistic insight into the origin of DGJ response precluding the formulation of alternative therapeutic approaches for nonresponsive mutants.

As discussed above, most Fabry disease mutants cause α-Gal misfolding and retrograde degradation (9, 11, 19), and aggregation of α-Gal in the ER has also been reported (20). Reumers *et al.* reported that certain types of mutations in α-Gal could give rise to increased protein aggregation propensity (21). Here, we have analyzed the impact of protein aggregation on the activity and DGJ response of Fabry disease mutants and showed that beyond mere misfolding, the tendency of misfolded α-Gal to aggregate (*i.e.* the formation of stable interactions between misfolded molecules) is an important determinant of mutant α-Gal activity and DGJ sensitivity. Using protein aggregation propensity as a measure of structural perturbation, rather than structural destabilization only, allows classifying DGJ-responsive mutants with accuracy similar to that of sequence-based methods but more importantly, provides a rationale to explain the lack of therapeutic response. This work shows that it is possible to quantify protein-specific proteostatic parameters determining the efficacy of pharmacological chaperones (22). It also suggests that the most severe Fabry disease mutants will not only benefit (23) but probably even require a therapeutic approach combining both pharmacological chaperones that stabilize the native fold and proteostatic regulators that can modulate the aggregation propensity of disease mutants *in vivo* (24).

EXPERIMENTAL PROCEDURES

In Silico Analysis of Aggregation, Stability, and Structure of α-Galactosidase and Fabry Disease Mutations—The aggregation propensities of α-Gal and its mutants were analyzed with TANGO (25), an algorithm to predict aggregation-nucleating sequences in proteins. For the analysis, the default parameters of the program were used. The effect of the mutations on α-Gal stability was analyzed by calculating the change in free energy ($\Delta\Delta G$) upon mutation with the FoldX 3.0 force field (26). The α-Gal structures were repaired using the RepairPDB command, and with the BuildModel command mutations were performed. Default parameters were used for the analysis. The set of 1331 validated polymorphisms from >50 proteins that were used for ΔΔG comparison is available in the supplemental table. The structural changes of α-Gal due to mutations were inspected with YASARA (27). SNPeffect is a publically available database for phenotyping human single nucleotide polymorphisms containing >60,000 human variants gathered from UniProt (28).

Plasmid Construction and Mutagenesis of α-Galactosidase—The full-length cDNA sequence encoding human α-Gal A (NM_000169) was cloned into the pcDNA4/TO/myc-His vector (Invitrogen). The insert was amplified using primers specific for the human α-Gal gene on Gene Pool cDNA template from human normal skeletal muscle (Invitrogen) with Phusion polymerase (Finnzymes). Then, the PCR product was digested with restriction enzymes HindIII and XhoI and cloned in pcDNA4/TO/myc-His vector to generate an open reading frame encoding α-Gal with a C-terminal Myc tag. Expression vectors containing single-mutated α-Gal (H46Y, D165V, P265R, D266V, D244N, M267I, A288D, M290I, P293T, M296I, D313Y, N320I, and R356W) were generated by site-directed mutagenesis using sequence-specific primers and PWO DNA polymerase (Roche Applied Science).

Cell Culture and Transient Transfection in HeLa Cells—Human cervical cancer cell line HeLa (used for maximum 20 passages) was cultured in DMEM/F12 medium (Invitrogen) supplemented with 10% FCS and 1% antibiotics (penicillin/streptomycin) at 37 °C in 5% CO_2. For transient transfection 350,000 HeLa cells were plated in 6-well culture plates per well in the medium without antibiotics. 1 μg of plasmid DNA (Myc-tagged wild type or mutated α-Gal) was transfected into HeLa cells using FuGENE HD transfection reagent (Roche Applied Science) according to the manufacturer's protocol. 48 h after transfection, cells were removed from the incubator and examined.

SDS-PAGE and Western Blotting—48 h after transfection HeLa cells were lysed in M-PER lysis buffer (Pierce) and fractionated by SDS-PAGE (NuPAGE system; Invitrogen). For SDS-PAGE the scraped cells were heated with 2% SDS buffer at 99 °C for 10 min, separated using a 10% Bis-Tris gel in MES running buffer, and subsequently transferred by electroblotting (fixed current 0.4 A) on a nitrocellulose membrane (Millipore). The membrane was incubated in 5% dried nonfat milk powder dissolved in 0.2% Tris-buffered saline-Tween (TBST) for 1 h at room temperature and subsequently incubated with primary mouse anti-Myc antibody (Invitrogen) followed by incubation with secondary goat HRP-conjugated anti-mouse IgG (Promega). Proteins were visualized using chemiluminescence immunoblotting detection reagent (ECL; Millipore).

Size Exclusion Chromatography (SEC)—For the analysis of the α-Gal aggregation state by SEC, transfected HeLa cells were lysed in radioimmune precipitation assay (RIPA) buffer (1% octylphenoxypolyethoxyethanol (IGEPAL), 0.5% sodium deoxycholate, and 0.1% sodium dodecyl sulfate (SDS)) (Pierce) supplemented with protease inhibitors (Roche Applied Science), centrifuged for 5 min at 3000 rpm, and 400 μl of the supernatant was subsequently loaded onto a Superdex S200 HR10/30 column (GE Healthcare) equilibrated in hypotonic buffer (20 mM HEPES, 10 mM KCl, 1 mM $MgCl_2$, 1 mM EDTA, 1 mM EGTA, 1 mM DTT, pH 7.5). Eluted fractions were concentrated by 20% trichloroacetic acid precipitation, washed with acetone, and analyzed by SDS-PAGE. The bands densities were quantified using Quantity One program from ChemiDoc System (Bio-Rad). A mixture of molecular mass markers (Bio-Rad) was injected onto the column as a gel filtration standard.

Enzymatic Assay—The activity of α-Gal was determined by fluorogenic substrate 4-methylumbelliferyl-α-D-galactopyranoside (5 mM 4-MU-α-Gal) as described previously (29). *N*-Acetylgalactosamine (D-GalNAc) was used as an inhibitor of α-Gal B activity. α-Gal B is a second α-galactosidase in the cells that hydrolyzes the artificial substrate, but its activity in FD patients is normal or increased. In brief, HeLa cells transfected with wild type or mutant α-Gal were harvested and lysed in phosphate-buffered saline, pH 7.4 (PBS), by three cycles of freezing/thawing in acetone-dry ice water bath. The supernatant obtained by centrifugation at 10,000 × *g* was incubated with substrate solution (5 mM 4-MU-α-Gal and 100 mM D-GalNAc in 0.1 M citrate buffer, pH 4.5) at 37 °C, and the fluorescence was measured in a plate reader (POLARstar OPTIMA; BMG Labtech) within an hour. The slope of the linear part of the substrate conversion curve was a measure of the concentration of active enzyme in the lysates. Additionally, α-Gal concentration in the whole cell lysates was determined by Western blotting. To determine the enzymatic activity, the assays were performed in three independent experiments.

Immunofluorescence—HeLa cells were transfected on glass coverslips previously covered with poly-L-lysine (Sigma) as described for the transient transfection paragraph. 48 h after transfection, the cells were washed in PBS, fixed with 4% formaldehyde (20 min, room temperature), permeabilized in 0.1% Triton X-100 in PBS (5 min, room temperature), and blocked (1 h, room temperature) in a blocking buffer (1% BSA, 10% goat serum, and 0.2% Triton X-100 in PBS). The primary antibodies for the Myc tag (Invitrogen), LAMP1 for lysosomal staining (Abcam), BiP for ER staining (Abcam), and Giantin for Golgi staining (Abcam) were diluted 1:200 in blocking buffer and incubated 1 h at room temperature (or overnight at 4 °C). The secondary antibodies (goat anti-mouse Alexa Fluor 488 or goat anti-rabbit Alexa Fluor 594) were diluted 1:400 and incubated for 1 h at room temperature. The coverslips were stained with DAPI (1:10,000) and mounted on a slide with antifade reagent (ProLong Gold Antifade Reagent; Invitrogen). The slides were examined under fluorescence (100× oil objective; ECLIPSE TE2000, Nikon, Japan) and confocal microscope (60× oil objective; EZ-C1, Nikon, Japan). The final image processing and co-localization analysis were done with ImageJ. For the localization studies in total 300 cells from three independent experiments were counted.

Chemical Chaperone Treatment—5 μM DGJ (Sigma) was added to the culture medium for 24 h incubation after transfection. 5 μg/ml brefeldin A (BFA) was added to the cells 3 h before harvesting. The cells were washed three times with PBS before harvesting. The increase of the activity was normalized against the nontreated HeLa cells.

Statistical Analysis—To confirm the consistency of the results, all described experiments were performed in three separate replicates. For statistical evaluation of the determined averages and S.D., data were analyzed for significant differences using paired Student's *t*-test with a p value < 0.05.

RESULTS

Mapping the Aggregation Profile of α-Galactosidase Mutants—The aggregation of a protein in a living cell is determined by both protein-dependent and environmental factors. Environmental factors include protein expression levels and the capacity of the protein quality control machinery to maintain proteostasis. Protein-dependent factors determining aggregation propensity include the conformational stability of the native state as well as the intrinsic aggregation propensity of the primary protein structure, *i.e.* the propensity of the unfolded protein chain to self-associate by nonnative interactions (Fig. 1*A*). This self-association into aggregates is geared by short aggregation-prone stretches within a protein sequence that assemble by forming nonnative β-strand-mediated interactions. When the protein is folded in the native state these aggregation-prone sequence segments are generally buried in the hydrophobic core and unavailable for aggregation. Disease mutants can therefore affect the aggregation propensity in two ways that are not mutually exclusive. A mutation can destabilize the native state, thereby increasing the accessibility of aggregation-prone sequence segments, or a mutation can occur within an aggregation-prone segment thereby increasing its intrinsic propensity to self-associate. In combination, a point mutant occurring within an aggregation-prone sequence can simultaneously increase the intrinsic aggregation propensity and destabilize the protein structure (Fig. 1*A*).

To map the spectrum of aggregation propensities in α-Gal mutants we analyzed the 222 publicly available Fabry disease mutations using both TANGO (25), an algorithm that evaluates the intrinsic aggregation propensity of a protein sequence, and FoldX (26) a force field that calculates the thermodynamic

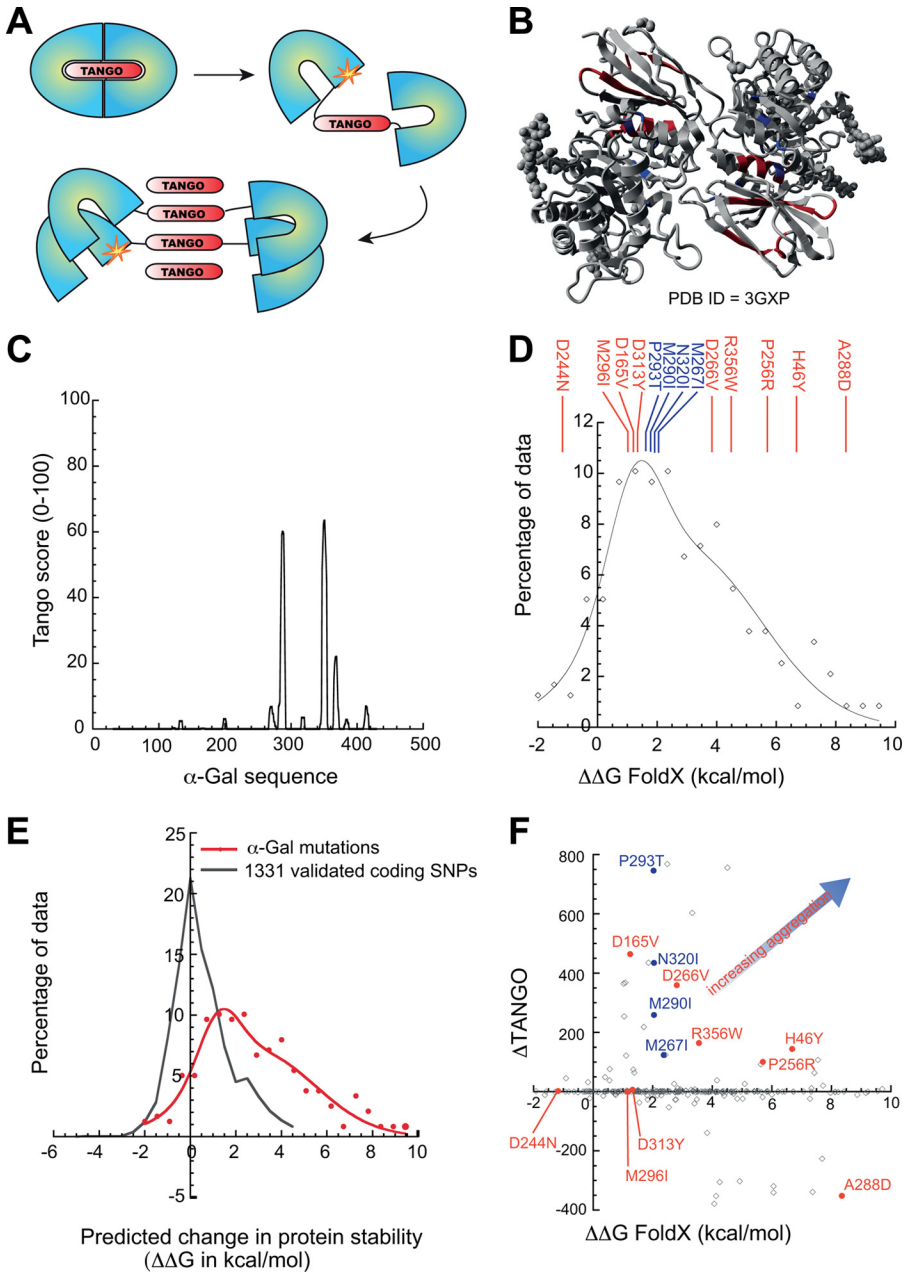

FIGURE 1. **Structure, stability, and aggregation propensity of human wild type α-Gal and Fabry-disease associated mutations.** *A*, schematic illustration of the general principle that protein aggregation is driven by specific short sequence stretches. Here we use the TANGO algorithm to identify these stretches (25). When the protein is natively folded, the aggregation prone sequences are buried inside its hydrophobic core. Conditions or mutations that lead to the destabilization of the native structure of the protein expose the aggregation prone stretches and thus promote aggregation. *B*, structure of human α-Gal A (Protein Data Bank ID 3GXP) (12) showing the functional homodimer. Each monomer consists of two domains: an α-β domain where the active site is located and an antiparallel β domain. The aggregation nucleating regions as predicted by TANGO are indicated in *red*. The structure was visualized with YASARA (27). *C*, intrinsic aggregation propensity of the α-Gal sequence as predicted by the TANGO algorithm revealing three strongly aggregation-prone regions with TANGO score above 20%: M^{284}ALWAIMA^{291}, L^{347}AWAVAMI^{355}, and Y^{365}TIAVAS^{371}. *D*, histogram of the thermodynamic stability change (ΔΔG in kcal/mol) associated with Fabry disease-causing mutations showing a broad distribution with a peak around 2.0 kcal/mol destabilization and a tail toward stronger destabilization, suggesting that the majority of disease α-Gal mutations have a destabilizing effect on the native structure. The mutant sets selected for the current study are indicated above in *red* and *blue*. *E*, comparison of the thermodynamic stability change (ΔΔ*G* in kcal/mol) associated with a set of validated polymorphisms from the Swissvar data base (*gray line*) with disease-associated mutations (*red line*). In contrast to the disease-associated mutations that display a peak around 2 kcal/mol destabilization, the polymorphism histogram displays a single distribution centered around 0 kcal/mol. *F*, MASS plot for all Fabry disease-associated α-Gal mutants, *i.e.* a scatter plot of the change of the thermodynamic stability (ΔΔ*G*) associated with mutation *versus* the corresponding change of intrinsic aggregation propensity (ΔTANGO). This scatter plot shows that the majority of the mutations do not affect the intrinsic aggregation propensity of the sequence, but rather increase aggregation by reducing the thermodynamic stability of the protein. The representative mutations used in this study are indicated in *red* and *blue*. The *blue arrow* indicates the direction of increasing aggregation propensity.

effect of mutations (change in free energy of unfolding ΔΔ*G* expressed in kcal/mol). α-Gal consists of two domains: an α-β domain where the active site is located and an antiparallel β domain (Fig. 1*B*). Analysis with the prediction algorithm TANGO reveals three strongly aggregation-prone sequences (Fig. 1*C*), located in the antiparallel β domain and the interface with the active site domain (indicated in *red* in Fig. 1*B*). The histogram of the ΔΔ*G* values for the 222 disease mutants eval-

uated by FoldX shown in Fig. 1*D* reveals a broad distribution with a clear peak near 2 kcal/mol destabilization and a long tail toward more severely destabilizing $\Delta\Delta G$ values. As the thermodynamic stability of most proteins is only marginal, with values commonly ranging from −5 to −10 kcal/mol, a mutation that causes destabilization of >2 kcal should be considered as very severe. For comparison we performed a similar analysis on a set of 1331 validated polymorphisms from the Swissvar database (30), affecting >50 proteins. The histogram of the corresponding $\Delta\Delta G$ values (Fig. 1*E*) displays a single distribution centered around 0 kcal/mol, confirming that most α-Gal mutations occurring in patients with Fabry disease detrimentally affect the thermodynamic stability of the protein. Consistent with the notion of loss of function of α-Gal in Fabry disease, several of the less destabilizing mutations act by altering the active site of the enzyme (data not shown). Reduction of the thermodynamic stability of a protein will increase the solvent exposure of aggregation prone regions (Fig. 1, *A–C*), thereby promoting aggregation. In addition, mutations may increase the aggregation propensity of the protein by increasing the intrinsic aggregation propensity, which can be revealed by the TANGO algorithm. As the intrinsic aggregation of a polypeptide sequence consists of a small number of short aggregation prone sequences and in contrast many residues cooperate to the thermodynamic stability of the native structure, it is expected that most mutations do not affect the TANGO score but increase aggregation via reduction of the stability. This is illustrated in a scatter plot of $\Delta\Delta G$ *versus* ΔTANGO values, further termed MASS plot (for Mutant Aggregation and Stability Spectrum) for all the mutants (Fig. 1*F*), which shows the majority of the mutations on the *x* axis (no change in TANGO), although mutations that alter the intrinsic aggregation propensity are not uncommon and generally consist of the mutation of charged residues that oppose aggregation (aggregation gatekeeper residues) (31). On a MASS plot the aggregation propensity of a protein will therefore increase with increasing intrinsic aggregation or decreasing thermodynamic stability, as indicated by the *blue arrow* (Fig. 1*F*).

Misfolding-associated versus Aggregation-associated Loss of Function—Based on the distribution on the MASS plot discussed above, we selected nine representative mutations that are spread right through the aggregation spectrum (indicated in *red* in Fig. 1, *D* and *F*) and transiently expressed these in HeLa. We characterized aggregation of wild type and mutant α-Gal by performing SEC on the lysates from transient transfection in HeLa cells, followed by SDS-PAGE of the fractions and Western blot analysis (Fig. 2, *A* and *B*). HeLa cells were lysed using RIPA buffer that contains 0.1% SDS, which can potentially break up unstable aggregates. Nevertheless, mutants with a severe decrease in thermodynamic stability or increase in intrinsic aggregation propensity, such as A288D ($\Delta\Delta G = 7.60$) and D165V (ΔTANGO = 464), respectively, eluted in the void volume, consistent with the formation of aggregates (Fig. 2, *A* and *B*). Wild type and mutants with small predicted changes in the thermodynamic stability and intrinsic aggregation values, such as M296I ($\Delta\Delta G = 1.71$, ΔTANGO = 0), eluted between 12 and 13 ml, corresponding to the dimeric active form of the protein. Further, we analyzed the enzymatic activity in lysates obtained from these cells (Fig. 2*C*), by following the conversion of an excess of the fluorogenic substrate 4-MU-α-Gal over time. Because under these conditions the enzyme is limiting and we do not consider mutations that directly affect the enzymatic mechanism, the slope of the linear part of the substrate conversion curve is a measure of the concentration of active enzyme in the lysates. Consistently, in the enzymatic assays, the aggregation-prone mutants showed negligible activity compared with wild type, whereas milder nonaggregating mutants such as M296I showed residual activity (Fig. 2*D*). Finally, we assessed the efficiency of translocation of the different α-Gal mutants to the lysosomes via ER and Golgi by immunofluorescence (Fig. 3*A*). Lysosomal localization was determined by co-localization with the lysosomal-associated membrane protein 1 (LAMP1), ER localization was determined by co-localization with the ER specific Hsp70 homolog BiP, and Golgi localization was determined by co-localization with the specific marker protein Giantin (Fig. 3*A*). This revealed that whereas wild type α-Gal is found throughout the ER, Golgi and in lysosomes, the mutants are found mainly in the ER and the Golgi, confirming that both misfolding and aggregation affect proper translocation (Fig. 3*B*). Although the details of the maturation process of the aggregating mutants remains to be clarified, the fact that they were retained in the ER suggests that most probably could not undergo the maturation process and pass the quality control systems there.

Together these data illustrate the variability in aggregation propensity of different α-Gal mutants showing that structural and functional effects range form simple misfolding-associated loss of function to aggregation-associated loss of function. Although these experiments have been performed under conditions of overexpression that might exacerbate aggregation, the observed relative differences in aggregation between the different mutants remain significant, as even under these conditions of high cellular α-Gal concentrations wild type and mild Fabry disease mutants do not aggregate.

A Scoring Function to Predict α-Gal Aggregation—Analysis of the nine mutants studied above suggests that mutants with a $\Delta\Delta G$ value larger than 3 kcal/mol (such as D266V, R356W, P265R, H46Y, and A288D) are systematically aggregation-prone, whereas mutants such as D244N, which is largely neutral in terms of thermodynamic stability and intrinsic aggregation, are largely soluble and usually retain some residual activity (provided the active site is not mutated). Interestingly, the situation is less well defined at destabilization values near 1.5–2.0 kcal/mol, which is where most α-Gal mutants cluster (Fig. 1*D*). Whereas mutants M296I ($\Delta\Delta G = 1.71$ kcal/mol) and D313Y ($\Delta\Delta G = 1.65$ kcal/mol) are still soluble and active, mutant D165V ($\Delta\Delta G = 1.51$ kcal/mol) is not. The positions of mutants M296I, D313Y, and D165V on the MASS plot (Fig. 1*F*) suggest the change in intrinsic aggregation seems to provide the answer here, as the aggregating mutant D165V displays a strong increase in TANGO value (ΔTANGO = 464). To confirm the notion that intrinsic aggregation propensity is the key determinant at a given value of protein stability, we selected four additional mutants that share similar $\Delta\Delta G$ values around 2 kcal/mol but display varying TANGO scores: M267I ($\Delta\Delta G = 2.45$, ΔTANGO = 121), M290I ($\Delta\Delta G = 2.12$, ΔTANGO = 254),

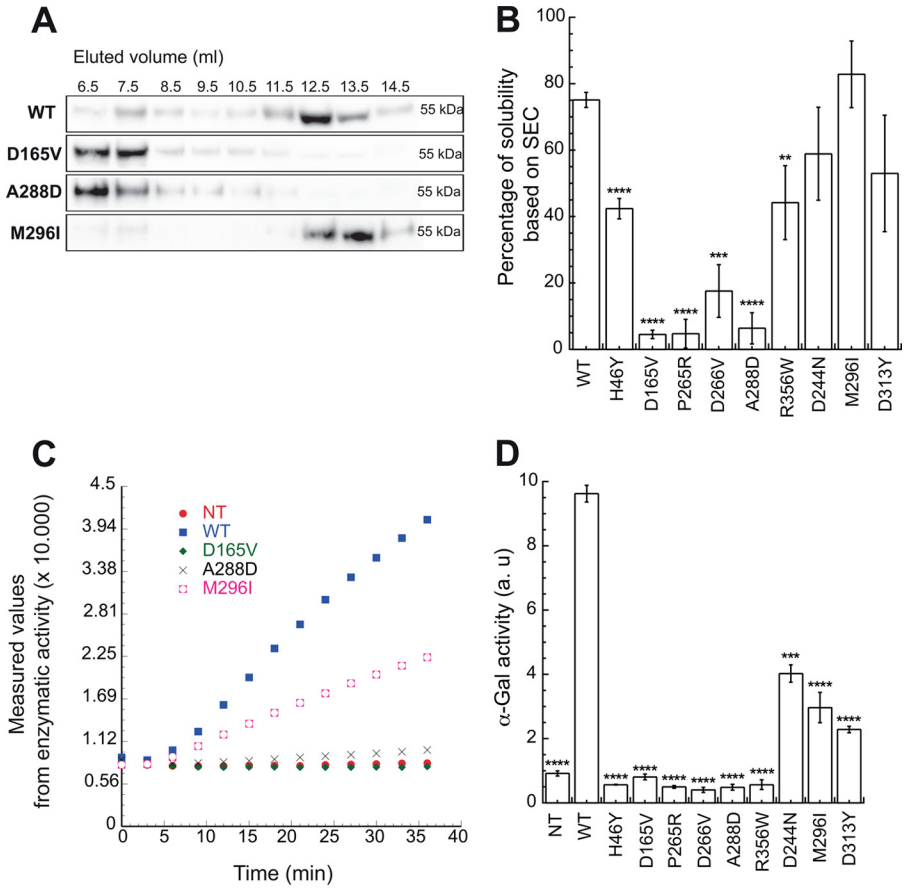

FIGURE 2. **Characterization of aggregation and enzymatic activity of α-Gal mutants.** *A*, Western blot of SEC fractions of wild type α-Gal and selected mutants in transiently transfected HeLa cells. WT α-Gal and M296I nonaggregating mutant eluted in later fractions (12.5–14.5 ml) than the aggregating mutants, corresponding to the soluble form of the protein. Aggregating α-Gal mutants such as D165V and A288D eluted in the column void volume (6.5–7.5 ml), indicating the presence of large protein assemblies of high molecular mass. *B*, quantification of the solubility of α-Gal mutants in transiently transfected HeLa cells. The bands densities from Western blot of SEC fractions from three experiments were quantified. Fractions from 6.5 to 10.5 ml elution were considered as insoluble whereas from 12.5 to 14.5 ml as soluble. Wild type α-Gal and M296I nonaggregating mutant were highly soluble (reaching approximately 80% of total solubility). Mutants such as H46Y, R356W, D24N, and D313Y were partially soluble whereas D165V, P265R, and A288D were nearly completely insoluble. *C*, representative kinetic curves of the enzymatic activity of α-Gal mutants followed by the conversion of the fluorogenic substrate 4-MU-α-Gal. *D*, quantification of the enzymatic activity of wild type α-Gal and selected disease-causing mutations in transiently transfected HeLa cells obtained by fitting the kinetic traces shown in *C*. Activity was completely lost for all aggregating mutants compared with wild type protein. Nonaggregating mutants (D244N, M296I, and D313Y) displayed some partial activity. The statistical significance of the decrease in solubility and activity is marked with *asterisks*: **, $p < 0.01$; ***, $p < 0.001$; and ****, $p < 0.0001$. Experimental data are mean ± S.D. (*error bars*) of three independent experiments.

N320I ($\Delta\Delta G$ = 2.12, ΔTANGO = 435), P293T ($\Delta\Delta G$ = 2.03, ΔTANGO = 756). We analyzed the aggregation propensity of these mutants upon transient transfection in HeLa cells by SEC as before (Fig. 4, *A* and *B*) and also measured the enzymatic activity in the lysates (Fig. 4*C*). As can be seen from the plot of solubility *versus* TANGO score (Fig. 4*D*), for mutants with similar $\Delta\Delta G$ values there is a clear trend for higher TANGO scores to correspond to increased experimental aggregation by SEC, confirming that both thermodynamic stability and intrinsic aggregation need to be combined to determine the aggregation tendency of the different mutants. Based on this, we proceeded to construct a simple scoring function that allows classifying aggregating *versus* nonaggregating mutants. This was achieved by adding an arbitrary penalty value of 5.0 to the $\Delta\Delta G$ value of each mutant that displayed a ΔTANGO value >100. As can be seen from Fig. 1*E*, a $\Delta\Delta G$ penalty of 5.0 kcal/mol corresponds to a severe thermodynamic destabilization that falls well outside the distribution observed for polymorphisms. Therefore, the effect of this penalty is to put mildly destabilized mutations that have a strong increase in intrinsic aggregation on par with mutants that are most severely destabilized. The ΔTANGO cut-off was estimated from the aggregation behavior in overexpression of the mutants with similar $\Delta\Delta G$ values in Fig. 4*B*. As can be observed in a plot of the relative enzymatic activity values (where 100% is wild type) *versus* the artificial score (Fig. 4*E*), the scoring function accurately separates active mutants from inactive ones.

Protein Aggregation Determines DGJ Response of α-Gal Disease Mutants—It was apparent from the SEC studies mentioned above that aggregated mutant α-Gal form stable nonnative structures, which are resistant to the detergents found in RIPA buffer. This suggests that a pharmacological chaperone such as DGJ, which relies on increasing native folding through binding to native structure (the active site), will have direct competition from nonnative interactions stabilizing α-Gal aggregates.

To establish to what extent protein aggregation affects the efficacy of treatment with DGJ, we determined the enzymatic activity of α-Gal in lysates of transiently transfected HeLa cells after treatment with 5 μM DGJ and plotted the increase in enzy-

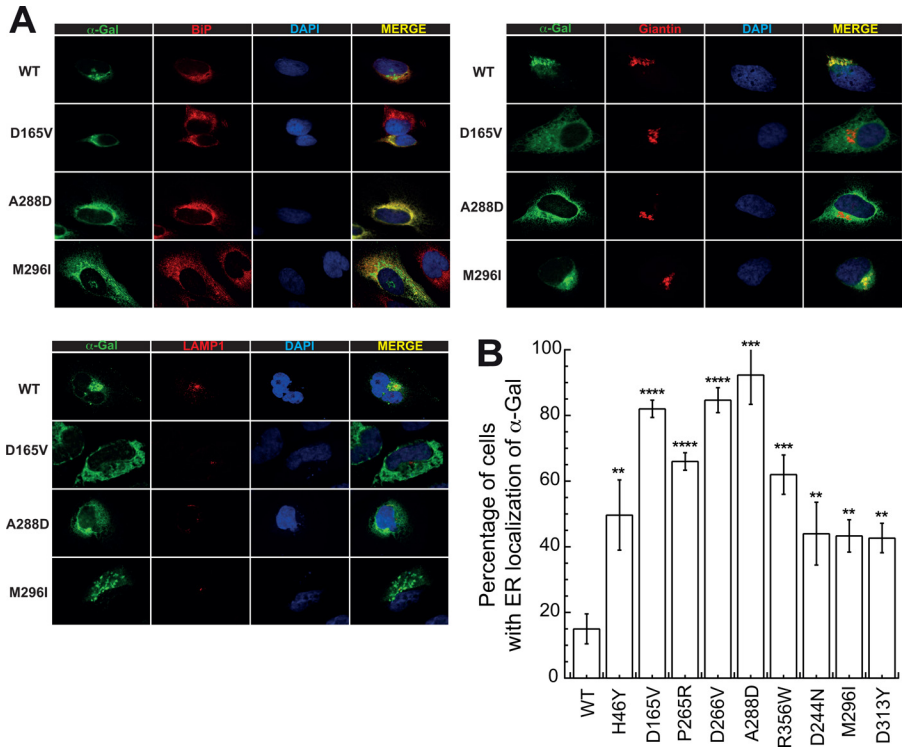

FIGURE 3. **Cellular processing of α-Gal mutants.** *A*, immunostaining of wild type and mutated α-Gal transiently expressed in HeLa cells and co-staining of cellular compartment markers: BiP (ER) Giantin (Golgi), and LAMP1 (lysosomes). α-Gal was stained in *green*, whereas the markers were visualized in *red*. The nuclei were stained with DAPI. α-Gal aggregating mutants D165V and A288D were localized predominantly in the ER, whereas WT and nonaggregating mutant M296I were localized mainly in the Golgi and lysosomes. *B*, quantification of the localization of wild type and disease mutants α-Gal in the ER. All aggregating α-Gal mutants were found predominantly in the ER, among which the A288D mutant was found in the ER in approximately 90% of counted cells. Nonaggregating mutants D244N, M296I, and D313Y were localized in the ER in 40% of counted cells. The statistical significance is marked with *asterisks*: **, $p < 0.01$; ***, $p < 0.001$; and ****, $p < 0.0001$. Experimental data are mean ± S.D. (*error bars*) of cell counting from three independent experiments.

matic activity upon treatment (relative to wild type) *versus* the solubility of the mutants in a scatter plot (Fig. 5*A*). Under these conditions we could observe limited DGJ response for the most soluble mutants only.

It has been shown that treatment of murine fibroblasts with BFA after preincubation with DGJ restores the turnover rate of the R301Q disease mutant to wild type levels (32). BFA is an antiviral metabolite from fungi (33) that interferes with anterograde transport from the endoplasmic reticulum to the Golgi apparatus leading to the retention of secretory proteins in the ER (34). As a result it will increase retrograde accumulation of both wild type and inactive mutant α-Gal from the Golgi to the ER. Inhibition of post-ER protein transport by BFA allows to normalize for intracellular trafficking and a more direct comparison of DGJ efficiency between different mutants. When BFA and DGJ treatments were combined, a strong synergistic response was observed for the more soluble mutants (Fig. 5, *B* and C). Although the amplitude of this response seems to scale with the solubility for mutants with a solubility of >50%, it is also clear that DGJ treatment is ineffective for the most insoluble proteins both alone or in combination with BFA.

To get a better understanding of the total impact of protein aggregation on DGJ response for Fabry disease patients, we turned to published DGJ responses of 75 α-Gal missense mutations in cultured lymphoblasts of Fabry disease patients (13). We employed these values, obtained under endogenous expression conditions, to test the ability of the scoring function that correctly predicts mutant α-Gal aggregation under overexpression to correctly classify DGJ responsive mutants from nonresponsive ones. We represent the results as a so-called receiver operator curve, which plots the percentage of true predictions *versus* the level of false positives (Fig. 5*D*). An ideal predictive curve will approximate the *y* axis (perfect true positive rate without false positives), whereas a random prediction will lie on the diagonal. Our analysis shows that aggregation propensity can be used with surprising accuracy to predict α-Gal activity in response to DGJ treatment in patient lymphoblasts. For instance, we can correctly predict almost 77.5% of the responding mutants while allowing only about 15% false positives, which represents a prediction accuracy (*i.e.* the ratio of correct positive and negative predictions over the total amount of data points) of >80%. Using the prediction value corresponding to this prediction precision, we estimate that about 35% of the 300 known missense α-Gal mutants are susceptible to protein aggregation, which will negatively affect DGJ response.

MASS Plot as a Predictive Tool for the Severity of Aggregating Mutants of Fabry Disease and Protein Aggregation in Other Proteinopathies—With the aim of investigating whether MASS plot values could be correlated to the severity of Fabry disease mutants, we plotted both classic (*i.e.* early onset and generally more severe) as well as variant (late onset and milder) mutants on a MASS plot. The results showed that the mutants found in patients with the classic form of FD were spread through the aggregation spectrum and had high TANGO values, whereas the ones responsible for the variant form were mainly lying on the *x* axis. The comparison of $\Delta\Delta G$ and ΔTANGO average val-

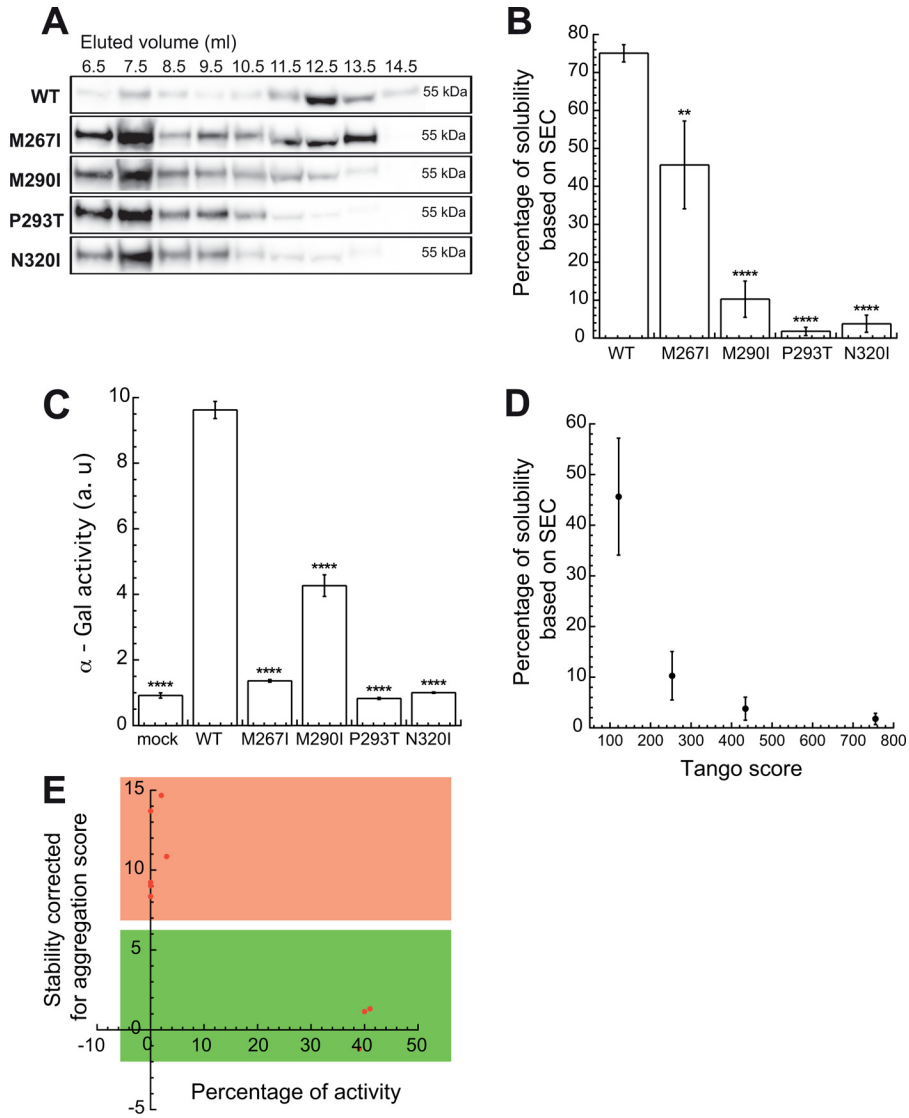

FIGURE 4. **Analyzing the effect of intrinsic aggregation propensity of the sequence at constant thermodynamic perturbation.** *A*, Western blot of SEC of wild type α-Gal and mutants selected to have similar $\Delta\Delta G$ values around 2 kcal/mol in transiently transfected HeLa cells. Mutants M267I and M290I were eluted both in the column void volume (6.5–7.5 ml) and in later fractions (8.5–13.5 ml), whereas mutants P293T and N320I were only eluted in the first fractions, indicating the presence of large protein assemblies of high molecular mass. *B*, quantification of the solubility by SEC of α-Gal mutants with a similar thermodynamic stability but increasing intrinsic aggregation propensity. *C*, quantified enzymatic activity of the additional α-Gal mutants. *D*, scatter plot of the quantified solubility by SEC *versus* the intrinsic aggregation propensity of the sequence according to TANGO. Higher TANGO scores correspond to lower solubility, *i.e.* increased aggregation. *E*, performance of the aggregation corrected protein stability score on the classification of α-Gal mutations in terms of their relative enzymatic activity. The aggregating mutants clustered together as the inactive group (*highlighted* in *red*), whereas the nonaggregating mutants were classified into the enzymatically active group (*highlighted* in *green*). The statistical significance is marked with *asterisks*: **, $p < 0.01$; and ****, $p < 0.0001$. Experimental data are mean ± S.D. (*error bars*) of three independent experiments.

ues for the two forms of FD showed that severe phenotype mutants had higher $\Delta\Delta G$ and ΔTANGO values than the less severe ones. Therefore, our results suggest that α-Gal aggregating mutants could lead to more rapid progress of FD.

Because there is an abundance of aggregation-prone sequences in the human proteome (21), we investigated the potential of MASS plot to evaluate and possibly classify the aggregation propensity of proteins responsible for various human diseases. In this manner we analyzed dozens of proteins with known structures responsible for different human disorders, and the results could be retrieved from the SNPeffect database (28). Representative examples are shown in Fig. 6. There is a clear spread between the mutations in the MASS plot, suggesting that such plots are useful to visualize the differences in aggregation properties of different mutants within a protein and can serve as a basis to analyze and classify aggregation-related phenotypes.

DISCUSSION

Approximately 50 lysosomal storage diseases have been described so far. Most of these disorders are loss-of-function diseases affecting a particular enzyme and are generally autosomal recessive or X-linked recessive as is Fabry disease. Lysosomal storage diseases are mostly the result of the inability of mutant proteins to fold efficiently and to be transported through the secretory pathway, resulting in ERAD of the mutant protein rather than translocation to the lysosome. Currently enzyme replacement therapy, in which wild type recom-

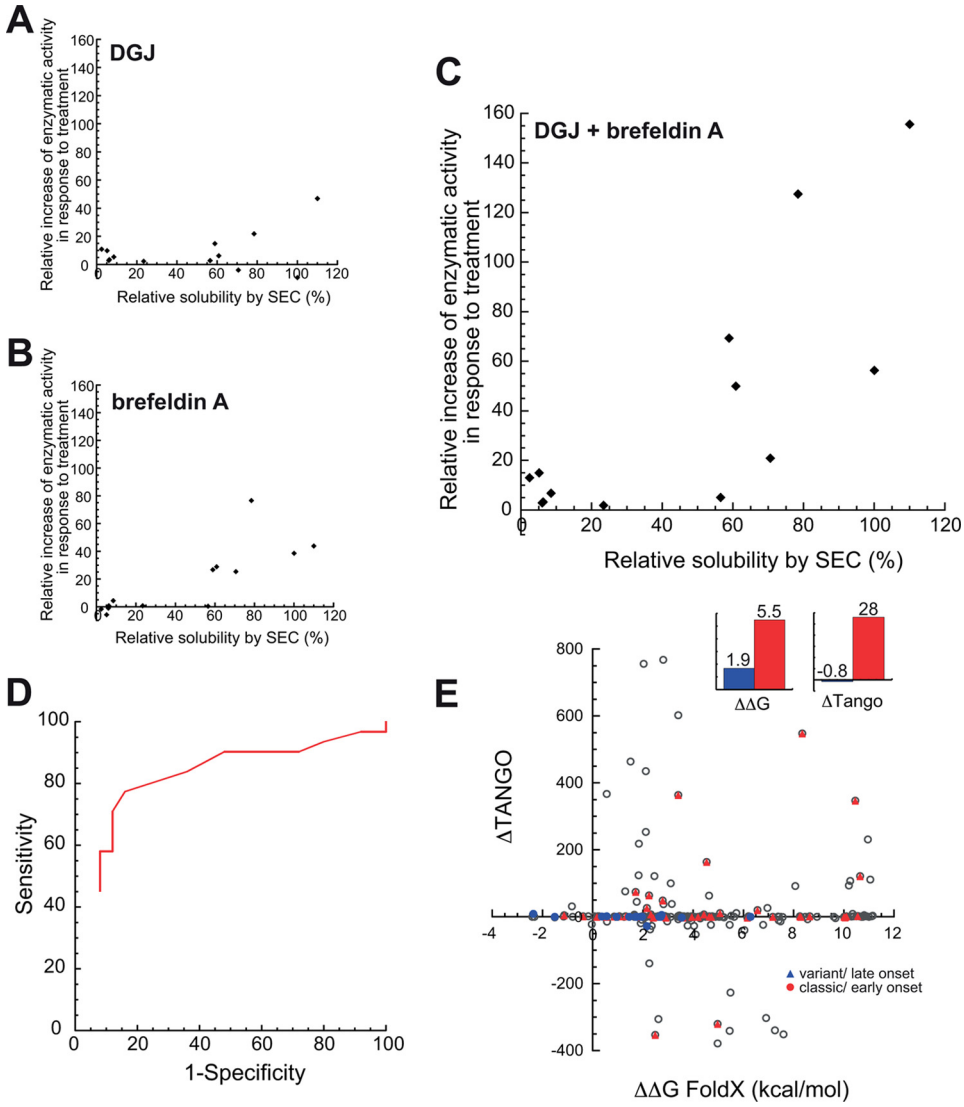

FIGURE 5. **Effect of aggregation on pharmacological chaperone response and disease severity.** *A*, treatment of HeLa cells transiently expressing α-Gal mutants with the pharmacological chaperone DGJ leads to an increase of the activity of mutants with a solubility measured by SEC of >50%. *B*, BFA treatment leads to an increase in enzymatic activity in HeLa cell lysates by α-Gal accumulation in the ER. *C*, synergistic effect of DGJ and BFA treatment results in a strong activation of soluble mutants but does not affect aggregating mutants. *D*, receiver operator curve displaying the accuracy of the aggregation-corrected protein stability score in predicting the response to DGJ treatment of α-Gal mutants in cultured lymphoblasts of Fabry disease patients (13). *E*, MASS plot of Fabry disease-associated α-Gal mutants with two groups of mutations severity. Mutations responsible for the classic form of Fabry disease are marked in *red*, whereas those responsible for the variant form are in *blue*. This scatter plot shows that the mutations causing the classic form of Fabry disease are spread out in the plot and have higher values of ΔΔ*G* and ΔTANGO compared with mutations causing the variant form of FD that are clustered in the *x* axis. The *bar charts* represent an average of ΔΔ*G* and ΔTANGO for the mutants belonging to each of the groups.

binant protein is intravenously supplied, is used for treatment of Gaucher disease, Fabry disease, glycogen storage disease type II (Pompe disease), and mucopolysaccharidosis I, II, and VI (35, 36). In parallel, pharmacological chaperone therapy, which contrary to enzyme replacement therapy is not restricted by the blood-brain barrier, is currently in development for Fabry disease, Gaucher disease, and Tay-Sachs disease (37–41). Although lysosomal storage diseases are largely monogenic diseases, these rare inherited disorders generally encompass a wide variety of familial variants ranging from mild to severe phenotypes. This is certainly the case for Fabry disease as >500 α-Gal mutations have been identified (42). As can be expected, this large variety of structural alterations also results in varying therapeutic response to the pharmacological chaperone DGJ (13). Structural analysis reveals that the most disruptive mutants are on average associated with the most severe forms of the disease, and they are also on average the least responsive to DGJ treatment (43, 44). However, it remains very difficult to predict DGJ response from structure only, as only 40% of the nonresponsive mutants can be identified in this manner (17, 18). Clearly, thermodynamic destabilization and thus severity of misfolding alone are not sufficient to characterize the therapeutic response (16).

Although Fabry disease is regarded as a misfolding disease caused by defective α-Gal that is eliminated by ERAD, some α-Gal mutants have been shown to be prone to form aggregates in which individual misfolded molecules interact to form cellular inclusions (20). Aggregation markedly changes the properties of the mutant proteins because aggregates are harder to degrade, induce changes in the expression of proteostatic net-

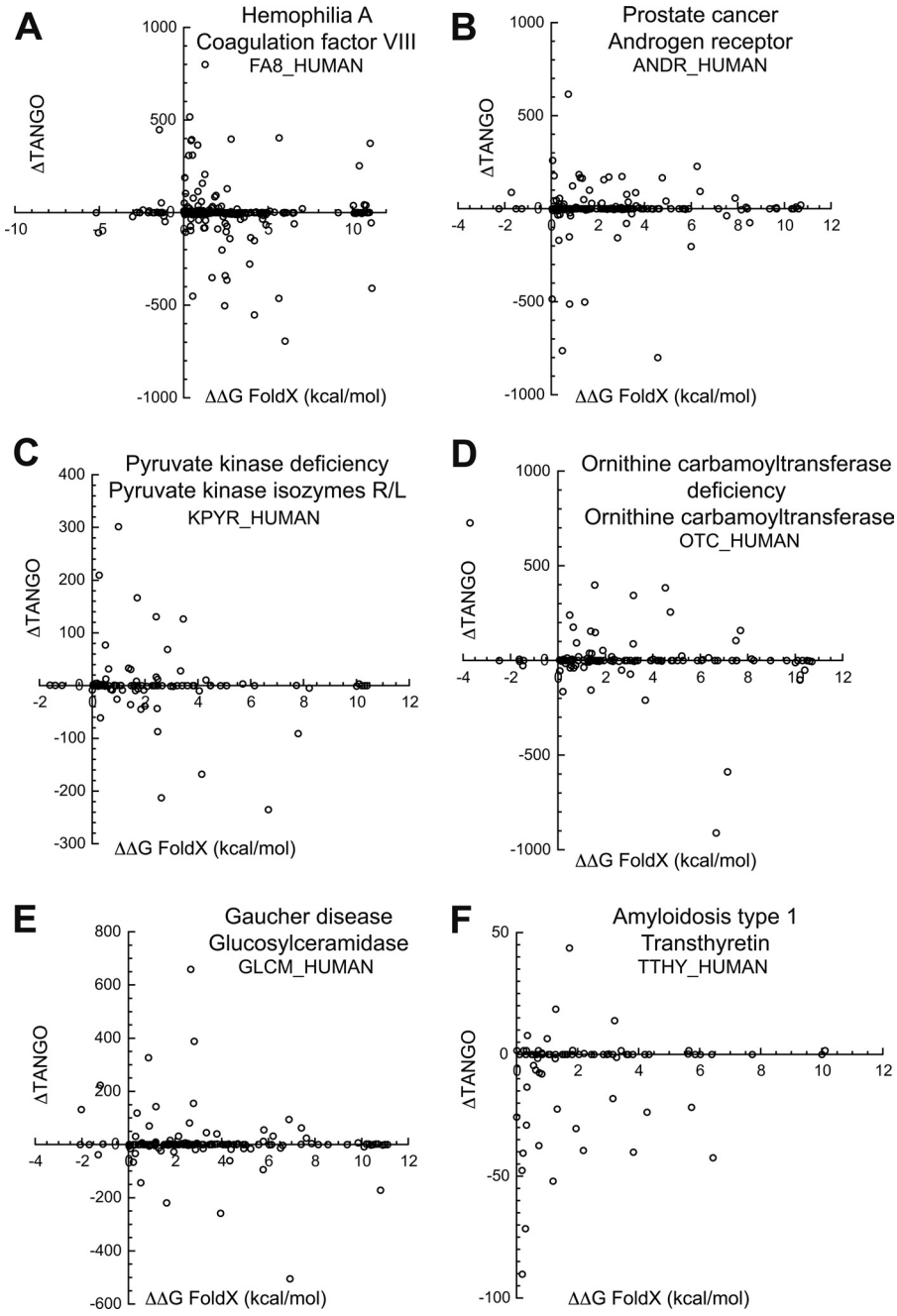

FIGURE 6. **MASS plot as a predictive tool for proteinopathies.** Scatter plots of the change of $\Delta\Delta G$ associated with mutation *versus* the corresponding change of ΔTANGO for hemophilia (*A*), prostate cancer (*B*), pyruvate kinase deficiency (*C*), ornithine carbamoyltransferase deficiency (*D*), Gaucher disease (*E*), and amyloidosis type 1 (*F*). These MASS plots show that certain disease mutations are spread through the aggregation spectrum, suggesting that they might affect the intrinsic aggregation propensity of the protein as well as reduce its thermodynamic stability, which could lead to protein aggregation.

work components, and may sequester essential cellular components. In our study we demonstrated that α-Gal aggregation could lead to more severe phenotypes because the aggregation-prone mutants could be correlated with the classic, more severe type of Fabry disease. Furthermore, α-Gal aggregation also correlated with qualitative differences in therapeutic response between merely misfolding mutants and aggregation-prone disease mutants. In an approach combining bioinformatic analysis with cell culture experiments, we found that rather than thermodynamic destabilization alone, the aggregation propensity of mutant α-Gal is a more reliable determinant of DGJ response. When presented to DGJ, misfolding-associated mutants can compensate structural defects by stabilizing DGJ/active site interactions, but in aggregated mutants these stabilizing interactions are in competition with nonnative interactions stabilizing the aggregate structure. Therefore, the aggregating α-Gal mutants seemed not to be amenable to DGJ treatment, which worked well for the mutants that do not have aggregating phenotype. When the categorization aggregated *versus* nonaggregated is applied to DGJ response data from earlier studies with patient-derived primary cell lines (13), we also find that DGJ efficiency is strongly affected by α-Gal aggrega-

tion, and using aggregation propensity as a classifier we can predict DGJ response with an accuracy that is equivalent to the most performing predictor algorithms using sequence information from α-Gal homologs (17, 18). This demonstrates that the aggregation propensity of α-Gal mutants is an important determinant for DGJ response, although it is clear that other factors certainly also participate. Apart from known active site disrupting mutants, other undetermined effects probably include more subtle conformational effects that alter the native state dynamics of the α-Gal structure or that affect structural regions that are not cooperatively connected to the active site (45, 46). Finally, our data reinforce the recent observation that additional strategies, such as the use of proteostatic regulators that can prevent aggregation, might be required to enhance the efficiency of chemical chaperones in lysosomal storage diseases (23).

REFERENCES

1. Brady, R. O., Gal, A. E., Bradley, R. M., Martensson, E., Warshaw, A. L., and Laster, L. (1967) Enzymatic defect in Fabry's disease: ceramidetrihexosidase deficiency. *N. Engl. J. Med.* **276,** 1163–1167
2. Ohshima, T., Murray, G. J., Swaim, W. D., Longenecker, G., Quirk, J. M., Cardarelli, C. O., Sugimoto, Y., Pastan, I., Gottesman, M. M., Brady, R. O., and Kulkarni, A. B. (1997) α-Galactosidase A-deficient mice: a model of Fabry disease. *Proc. Natl. Acad. Sci. U.S.A.* **94,** 2540–2544
3. Eng, C. M., and Desnick, R. J. (1994) Molecular basis of Fabry disease: mutations and polymorphisms in the human α-galactosidase A gene. *Hum. Mutat.* **3,** 103–111
4. Lemansky, P., Bishop, D. F., Desnick, R. J., Hasilik, A., and von Figura, K. (1987) Synthesis and processing of α-galactosidase A in human fibroblasts: evidence for different mutations in Fabry disease. *J. Biol. Chem.* **262,** 2062–2065
5. Garman, S. C., and Garboczi, D. N. (2004) The molecular defect leading to Fabry disease: structure of human α-galactosidase. *J. Mol. Biol.* **337,** 319–335
6. Schiffmann, R., Kopp, J. B., Austin, H. A., 3rd, Sabnis, S., Moore, D. F., Weibel, T., Balow, J. E., and Brady, R. O. (2001) Enzyme replacement therapy in Fabry disease: a randomized controlled trial. *JAMA* **285,** 2743–2749
7. Eng, C. M., Banikazemi, M., Gordon, R. E., Goldman, M., Phelps, R., Kim, L., Gass, A., Winston, J., Dikman, S., Fallon, J. T., Brodie, S., Stacy, C. B., Mehta, D., Parsons, R., Norton, K., O'Callaghan, M., and Desnick, R. J. (2001) A phase 1/2 clinical trial of enzyme replacement in Fabry disease: pharmacokinetic, substrate clearance, and safety studies. *Am. J. Hum. Genet.* **68,** 711–722
8. Desnick, R. J., Brady, R., Barranger, J., Collins, A. J., Germain, D. P., Goldman, M., Grabowski, G., Packman, S., and Wilcox, W. R. (2003) Fabry disease, an under-recognized multisystemic disorder: expert recommendations for diagnosis, management, and enzyme replacement therapy. *Ann. Intern. Med.* **138,** 338–346
9. Yam, G. H., Zuber, C., and Roth, J. (2005) A synthetic chaperone corrects the trafficking defect and disease phenotype in a protein misfolding disorder. *FASEB J.* **19,** 12–18
10. Yam, G. H., Bosshard, N., Zuber, C., Steinmann, B., and Roth, J. (2006) Pharmacological chaperone corrects lysosomal storage in Fabry disease caused by trafficking-incompetent variants. *Am. J. Physiol. Cell Physiol.* **290,** C1076–1082
11. Fan, J. Q., and Ishii, S. (2007) Active-site-specific chaperone therapy for Fabry disease: yin and yang of enzyme inhibitors. *FEBS J.* **274,** 4962–4971
12. Lieberman, R. L., D'aquino J. A., Ringe, D., and Petsko, G. A. (2009) Effects of pH and iminosugar pharmacological chaperones on lysosomal glycosidase structure and stability. *Biochemistry* **48,** 4816–4827
13. Benjamin, E. R., Flanagan, J. J., Schilling, A., Chang, H. H., Agarwal, L., Katz, E., Wu, X., Pine, C., Wustman, B., Desnick, R. J., Lockhart, D. J., and Valenzano, K. J. (2009) The pharmacological chaperone 1-deoxygalactonojirimycin increases α-galactosidase A levels in Fabry patient cell lines. *J. Inher. Metab. Dis.* **32,** 424–440
14. Sugawara, K., Ohno, K., Saito, S., and Sakuraba, H. (2008) Structural characterization of mutant α-galactosidases causing Fabry disease. *J. Hum. Genet.* **53,** 812–824
15. Matsuzawa, F., Aikawa, S., Doi, H., Okumiya, T., and Sakuraba, H. (2005) Fabry disease: correlation between structural changes in α-galactosidase, and clinical and biochemical phenotypes. *Hum. Genet.* **117,** 317–328
16. Shin, S. H., Kluepfel-Stahl, S., Cooney, A. M., Kaneski, C. R., Quirk, J. M., Schiffmann, R., Brady, R. O., and Murray, G. J. (2008) Prediction of response of mutated α-galactosidase A to a pharmacological chaperone. *Pharmacogenet. Genomics* **18,** 773–780
17. Andreotti, G., Guarracino, M. R., Cammisa, M., Correra, A., and Cubellis, M. V. (2010) Prediction of the responsiveness to pharmacological chaperones: lysosomal human α-galactosidase, a case of study. *Orphanet J. Rare Dis.* **5,** 36
18. Andreotti, G., Citro, V., De Crescenzo, A., Orlando, P., Cammisa, M., Correra, A., and Cubellis, M. V. (2011) Therapy of Fabry disease with pharmacological chaperones: from *in silico* predictions to *in vitro* tests. *Orphanet J. Rare Dis.* **6,** 66
19. Yam, G. H., Roth, J., and Zuber, C. (2007) 4-Phenylbutyrate rescues trafficking incompetent mutant α-galactosidase A without restoring its functionality. *Biochem. Biophys. Res. Commun.* **360,** 375–380
20. Ishii, S., Kase, R., Okumiya, T., Sakuraba, H., and Suzuki, Y. (1996) Aggregation of the inactive form of human α-galactosidase in the endoplasmic reticulum. *Biochem. Biophys. Res. Commun.* **220,** 812–815
21. Reumers, J., Maurer-Stroh, S., Schymkowitz, J., and Rousseau, F. (2009) Protein sequences encode safeguards against aggregation. *Hum. Mutat.* **30,** 431–437
22. Powers, E. T., Morimoto, R. I., Dillin, A., Kelly, J. W., and Balch, W. E. (2009) Biological and chemical approaches to diseases of proteostasis deficiency. *Annu. Rev. Biochem.* **78,** 959–991
23. Mu, T. W., Ong, D. S., Wang, Y. J., Balch, W. E., Yates, J. R., 3rd, Segatori, L., and Kelly, J. W. (2008) Chemical and biological approaches synergize to ameliorate protein-folding diseases. *Cell* **134,** 769–781
24. Ong, D. S., and Kelly, J. W. (2011) Chemical and/or biological therapeutic strategies to ameliorate protein misfolding diseases. *Curr. Opin. Cell Biol.* **23,** 231–238
25. Fernandez-Escamilla, A. M., Rousseau, F., Schymkowitz, J., and Serrano, L. (2004) Prediction of sequence-dependent and mutational effects on the aggregation of peptides and proteins. *Nat. Biotechnol.* **22,** 1302–1306
26. Schymkowitz, J., Borg, J., Stricher, F., Nys, R., Rousseau, F., and Serrano, L. (2005) The FoldX web server: an online force field. *Nucleic Acids Res.* **33,** W382–388
27. Krieger, E., Koraimann, G., and Vriend, G. (2002) Increasing the precision of comparative models with YASARA NOVA: a self-parameterizing force field. *Proteins* **47,** 393–402
28. De Baets, G., Van Durme, J., Reumers, J., Maurer-Stroh, S., Vanhee, P., Dopazo, J., Schymkowitz, J., and Rousseau, F. (2012) SNPeffect 4.0: on-line prediction of molecular and structural effects of protein-coding variants. *Nucleic Acids Res.* **40,** D935–939
29. Mayes, J. S., Scheerer, J. B., Sifers, R. N., and Donaldson, M. L. (1981) Differential assay for lysosomal α-galactosidases in human tissues and its application to Fabry's disease. *Clin. Chim. Acta* **112,** 247–251
30. Yip, Y. L., Famiglietti, M., Gos, A., Duek, P. D., David, F. P., Gateau, A., and Bairoch, A. (2008) Annotating single amino acid polymorphisms in the UniProt/Swiss-Prot knowledgebase. *Hum. Mutat.* **29,** 361–366
31. Rousseau, F., Serrano, L., and Schymkowitz, J. W. (2006) How evolutionary pressure against protein aggregation shaped chaperone specificity. *J. Mol. Biol.* **355,** 1037–1047
32. Hamanaka, R., Shinohara, T., Yano, S., Nakamura, M., Yasuda, A., Yokoyama, S., Fan, J. Q., Kawasaki, K., Watanabe, M., and Ishii, S. (2008) Rescue of mutant α-galactosidase A in the endoplasmic reticulum by 1-deoxygalactonojirimycin leads to trafficking to lysosomes. *Biochim. Biophys. Acta* **1782,** 408–413
33. Tamura, G., Ando, K., Suzuki, S., Takatsuki, A., and Arima, K. (1968) Antiviral activity of brefeldin A and verrucarin A. *J. Antibiot.* **21,** 160–161
34. Klausner, R. D., Donaldson, J. G., and Lippincott-Schwartz, J. (1992) Brefeldin A: insights into the control of membrane traffic and organelle

structure. *J. Cell Biol.* **116,** 1071–1080
35. Brady, R. O. (2006) Enzyme replacement for lysosomal diseases. *Annu. Rev. Med.* **57,** 283–296
36. Bruni, S., Loschi, L., Incerti, C., Gabrielli, O., and Coppa, G. V. (2007) Update on treatment of lysosomal storage disease. *Acta Myol.* **26,** 87–92
37. Asano, N., Ishii, S., Kizu, H., Ikeda, K., Yasuda, K., Kato, A., Martin, O. R., and Fan, J. Q. (2000) *In vitro* inhibition and intracellular enhancement of lysosomal α-galactosidase A activity in Fabry lymphoblasts by 1-deoxygalactonojirimycin and its derivatives. *Eur. J. Biochem.* **267,** 4179–4186
38. Matsuda, J., Suzuki, O., Oshima, A., Yamamoto, Y., Noguchi, A., Takimoto, K., Itoh, M., Matsuzaki, Y., Yasuda, Y., Ogawa, S., Sakata, Y., Nanba, E., Higaki, K., Ogawa, Y., Tominaga, L., Ohno, K., Iwasaki, H., Watanabe, H., Brady, R. O., and Suzuki, Y. (2003) Chemical chaperone therapy for brain pathology in G_{M1}-gangliosidosis. *Proc. Natl. Acad. Sci. U.S.A.* **100,** 15912–15917
39. Sawkar, A. R., Adamski-Werner, S. L., Cheng, W. C., Wong, C. H., Beutler, E., Zimmer, K. P., and Kelly, J. W. (2005) Gaucher disease-associated glucocerebrosidases show mutation-dependent chemical chaperoning profiles. *Chem. Biol.* **12,** 1235–1244
40. Sawkar, A. R., D'Haeze, W., and Kelly, J. W. (2006) Therapeutic strategies to ameliorate lysosomal storage disorders: a focus on Gaucher disease. *Cell Mol. Life Sci.* **63,** 1179–1192
41. Parenti, G. (2009) Treating lysosomal storage diseases with pharmacological chaperones: from concept to clinics. *EMBO Mol. Med.* **1,** 268–279
42. Schiffmann, R. (2009) Fabry disease. *Pharmacol. Ther.* **122,** 65–77
43. Garman, S. C., and Garboczi, D. N. (2002) Structural basis of Fabry disease. *Mol. Genet. Metab.* **77,** 3–11
44. Sugawara, K., Saito, S., Sekijima, M., Ohno, K., Tajima, Y., Kroos, M. A., Reuser, A. J., and Sakuraba, H. (2009) Structural modeling of mutant α-glucosidases resulting in a processing/transport defect in Pompe disease. *J. Hum. Genet.* **54,** 324–330
45. Freire, E. (1999) The propagation of binding interactions to remote sites in proteins: analysis of the binding of the monoclonal antibody D1.3 to lysozyme. *Proc. Natl. Acad. Sci. U.S.A.* **96,** 10118–10122
46. Lenaerts, T., Ferkinghoff-Borg, J., Stricher, F., Serrano, L., Schymkowitz, J. W., and Rousseau, F. (2008) Quantifying information transfer by protein domains: analysis of the Fyn SH2 domain structure. *BMC Struct. Biol.* **8,** 43